

Dimer Physics in the Frustrated Cairo Pentagonal Antiferromagnet $\text{Bi}_2\text{Fe}_4\text{O}_9$ K. Beauvois,^{1,2,*} V. Simonet,^{2,†} S. Petit,³ J. Robert,² F. Bourdarot,¹ M. Gospodinov,⁴ A. A. Mukhin,⁵ R. Ballou,^{1b,2}
V. Skumryev,^{6,7} and E. Ressouche¹¹*Université Grenoble Alpes, CEA, IRIG, MEM, MDN, 38000 Grenoble, France*²*Institut Néel, CNRS and Université Grenoble Alpes, 38000 Grenoble, France*³*Laboratoire Léon Brillouin, CEA-CNRS, Université Paris-Saclay, CE-Saclay, 91191 Gif sur Yvette, France*⁴*Institute of Solid State Physics, Bulgarian Academy of Sciences, 1184 Sofia, Bulgaria*⁵*Prokhorov General Physics Institute, Russian Academy of Sciences, 119991 Moscow, Russia*⁶*Departament de Física, Universitat Autònoma de Barcelona, 08193 Bellaterra, Barcelona, Spain*⁷*Institució Catalana de Recerca i Estudis Avançats, 08010 Bellaterra, Barcelona, Spain*(Received 12 September 2019; revised manuscript received 13 January 2020;
accepted 28 February 2020; published 24 March 2020)

The research field of magnetic frustration is dominated by triangle-based lattices but exotic phenomena can also be observed in pentagonal networks. A peculiar noncollinear magnetic order is indeed known to be stabilized in $\text{Bi}_2\text{Fe}_4\text{O}_9$ materializing a Cairo pentagonal lattice. We present the spin wave excitations in the magnetically ordered state, obtained by inelastic neutron scattering. They reveal an unconventional excited state related to local precession of pairs of spins. The magnetic excitations are then modeled to determine the superexchange interactions for which the frustration is indeed at the origin of the spin arrangement. This analysis unveils a hierarchy in the interactions, leading to a paramagnetic state (close to the Néel temperature) constituted of strongly coupled dimers separated by much less correlated spins. This produces two types of response to an applied magnetic field associated with the two nonequivalent Fe sites, as observed in the magnetization distributions obtained using polarized neutrons.

DOI: [10.1103/PhysRevLett.124.127202](https://doi.org/10.1103/PhysRevLett.124.127202)

Magnetic frustration, expected to occur when all spin pair interactions cannot be simultaneously satisfied, is one of the major ingredients at the origin of the flurry of discoveries in magnetic studies for the last 20 years. One of the basic experimental signatures of frustration is the difficulty of a system to order magnetically in spite of significant magnetic interactions, the extreme case being the absence of magnetic order at zero temperature as a consequence of the macroscopic degeneracy of the ground state [1–4]. In materials where the magnetic moments order eventually at finite temperature, this leads, in the region above the ordering temperature, but well below the temperature characterizing the strength of the interactions, to a classical spin liquid state, also called cooperative paramagnetic, where the magnetic moments are highly correlated although fluctuating. This disordered state can sustain not only well-defined excitations [5], but also zero energy modes, which are the signature of local motions connecting the ground-state spin configurations. These modes acquire a gap on entering the ordered phase [6] and are alternatively described in a molecular approach [7]. This rich physics has been well established for triangle-based lattices, for instance, the Heisenberg kagome antiferromagnet with nearest-neighbor interactions [5,8]. Many other exotic manifestations of magnetic frustration have been revealed in quantum systems or with additional ingredients, such as strongly anisotropic Hamiltonians [9–11].

Another direction has been opened with the identification of an equivalent for the pentagonal Cairo lattice in the real material $\text{Bi}_2\text{Fe}_4\text{O}_9$ [12]. The Cairo lattice is not based on triangles but on edge-sharing pentagons. It is then still prone to magnetic frustration due to the odd number of bonds in the elementary pentagonal units. This pentagonal lattice has a complex connectivity with three- and fourfold connected sites at variance with triangle-based lattices, which fosters alternative ways to accommodate frustration. This leads in $\text{Bi}_2\text{Fe}_4\text{O}_9$ to an unconventional ground state consisting of an orthogonal arrangement of the magnetic moments. This classical ground state was also obtained theoretically, as well as other interesting phases, including, in the presence of quantum fluctuations, a resonating valence bond liquid or an orthogonal dimer ground state (valence bond crystal) [13,14]. The latter recalls the exactly solvable dimer ground state of the Shastry-Sutherland lattice [15], largely investigated for its exotic physics [16,17]. These findings stimulated further theoretical [18–24] and experimental [25–28] studies on pentagon-based physics, even spreading beyond the field of magnetism. In spite of this interest, an experimental determination of the Hamiltonian of the prototypical material $\text{Bi}_2\text{Fe}_4\text{O}_9$ has never been reported yet that would solely ascertain the crucial influence of frustration on its exotic properties.

In this Letter, we present the experimental determination of the magnetic interactions in $\text{Bi}_2\text{Fe}_4\text{O}_9$, materializing a Cairo lattice with spins $5/2$ using inelastic neutron scattering. A minimum of five exchange interactions allows us to account for the magnetic order and for the associated excitations, including a peculiar quasiflat mode. We also show the magnetic density maps measured using polarized neutron scattering under a magnetic field. They reveal a correlated state above the ordering temperature, resulting from the hierarchy of interactions and characteristics of the underlying dimer physics.

The unit cell of the orthorhombic oxide $\text{Bi}_2\text{Fe}_4\text{O}_9$ contains eight magnetic Fe^{3+} ions equally distributed on two different Wyckoff sites of the $Pbam$ space group: $4h$ for Fe_1 and $4f$ for Fe_2 . These sites have a different connectivity and different oxygen coordination: tetrahedral for Fe_1 and octahedral for Fe_2 . They form a lattice closely related to the Cairo pentagonal one with noticeable differences (see Fig. 1): the site with fourfold connectivity in the perfect lattice is actually constituted by a pair of Fe_2 atoms located below and above the pentagonal plane. The projected lattice in the ab plane is also slightly distorted compared to the perfect Cairo lattice, as far as the bond lengths and bond angles are concerned. The Heisenberg Hamiltonian with isotropic exchange interactions is a good starting point to describe the magnetic properties of this frustrated lattice of Fe^{3+} ions ($J = S = 5/2$, $L = 0$),

$$\mathcal{H} = \sum_{\langle i,j \rangle} J_{ij} \mathbf{S}_i \cdot \mathbf{S}_j, \quad (1)$$

where \mathbf{S}_i is a spin operator and $J_{ij} = J_1 - J_5$ are the five superexchange interactions between pairs of spins, inferred from the structure [12]. There are three exchange couplings in the ab plane (J_3 , J_4 , and J_5) and two additional ones out of the plane of the pentagons (J_1 and J_2), which connect only the stacked Fe_2 [see Fig. 1(b)]. $\text{Bi}_2\text{Fe}_4\text{O}_9$ exhibits below $T_N \sim 240$ K a long-range antiferromagnetic order characterized by a propagation vector $\vec{k} = (1/2, 1/2, 1/2)$. The resulting spin configuration was elucidated by neutron diffraction (see Fig. 1) and is made of two sets of orthogonal pairs of antiferromagnetic spins in the ab plane corresponding to each Fe site, with a global rotation by an angle $\alpha = 155^\circ$ relative to each other [12]. Despite the deviation of the experimental system from the perfect Cairo lattice, this orthogonal magnetic structure matches the one identified in theoretical studies on the perfect lattice and is shown to be rather robust while varying the ratio of the exchange interactions and increasing the quantum fluctuations [14]. This peculiar magnetic structure actually results from both frustration and complex connectivity.

All our experiments were performed on a single crystal of $\text{Bi}_2\text{Fe}_4\text{O}_9$ of dimensions $\sim 2.5 \times 2 \times 1.5$ mm³, grown by the high flux temperature solution method using a flux of Bi_2O_3 . The magnetization distributions were obtained from two neutron scattering experiments performed on the CRG

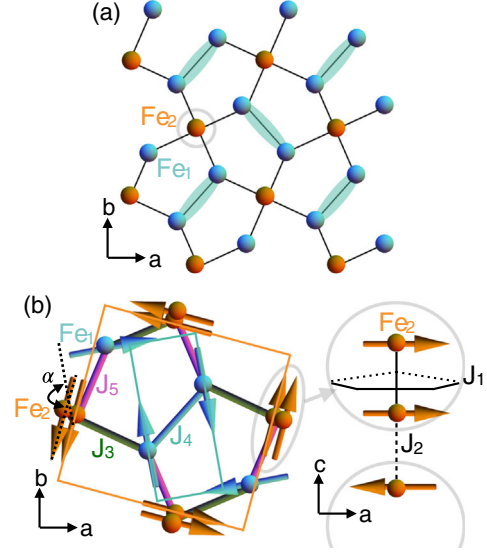


FIG. 1. (a) ab plane projection of the Fe atoms in $\text{Bi}_2\text{Fe}_4\text{O}_9$ forming an equivalent of the Cairo pentagonal lattice. The Fe_1 (in blue) and Fe_2 (in orange) have a different connectivity. Blue ellipses underline strongly coupled antiferromagnetic Fe_1 spins. (b) Magnetic arrangement stabilized below T_N : the orange and blue rectangles materialize the two sets of orthogonal antiferromagnetic pairs in the ab plane [12]. The Fe_2 form ferromagnetic pairs, sandwiching the Fe_1 planes. The five exchange interactions within and between the pentagonal planes are labeled.

D23 two-axis diffractometer at Institut Laue Langevin (ILL) in its polarized neutron mode, with an incoming neutron wavelength $\lambda = 2.37$ Å from a graphite-Heusler double monochromator configuration. Measurements were performed with a magnetic field of 6 T applied along the sample c axis at $T = 250$ K (paramagnetic state) and along the a - b crystallographic direction at $T = 250$ and 15 K (ordered state) (see Supplemental Material [29]). Inelastic neutron scattering (INS) experiments were performed on the CRG IN22 triple-axis spectrometer at ILL in an orange cryostat at a constant final wave vector $k_f = 2.662$ Å⁻¹, with an energy resolution equal to about 1 meV. The sample was oriented in order to access the (h, h, ℓ) scattering plane.

In order to measure the magnetic excitations, several constant- \mathbf{Q} energy scans have been performed at 1.5 K along the reciprocal space directions $(1/2, 1/2, \ell)$, $(h, h, 0)$, and $(2, 2, \ell)$ sketched in Fig. 2(a). The excitations along $(2, 2, \ell)$ were fitted using the TAKIN software [35,36], which includes the spin wave model as input and the instrument resolution [see Fig. 2(b)] (see Supplemental Material [29]). This treatment was necessary to disentangle two overlapping modes. The excitations in the other two directions were simply fitted by the sum of two Lorentz functions,

$$S(\mathbf{Q}, \omega) = bg + A(\omega, T) \left(\frac{1}{(\omega - \epsilon)^2 + \sigma^2} + \frac{1}{(\omega + \epsilon)^2 + \sigma^2} \right), \quad (2)$$

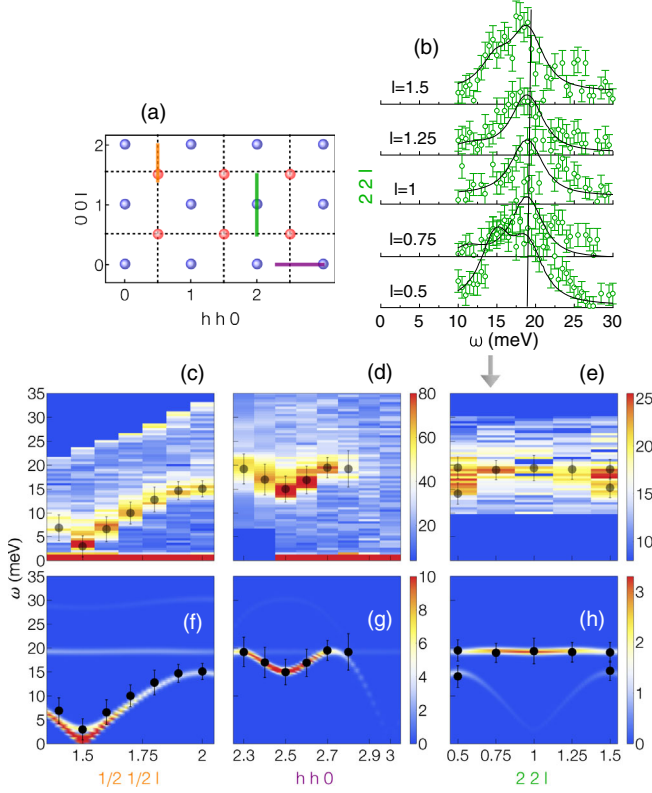


FIG. 2. (a) Sketch of the scattering plane (h, h, ℓ) investigated by INS in $\text{Bi}_2\text{Fe}_4\text{O}_9$, with the nuclear (blue spheres) and magnetic (red spheres) Bragg peak positions and the measurement cuts along the $(1/2, 1/2, \ell)$, $(h, h, 0)$, and $(2, 2, \ell)$ reciprocal space directions. (b) Along $(2, 2, \ell)$, series of measured constant- \mathbf{Q} energy scans and fit of the excitations (black lines). Measured (c)–(e) and calculated (f)–(h) dynamic structure factor $S(\mathbf{Q}, \omega)$ using the exchange constants of Table I and a small single-ion anisotropy term constraining the spins in the ab plane. The color scale of the calculations was truncated for the spectra along $(1/2, 1/2, \ell)$, $(h, h, 0)$ in order to emphasize the weaker flat mode along $(2, 2, \ell)$. The width of the calculated excitations was taken as the energy resolution of 1 meV. The empty (filled) black points on top of the measured (calculated) $S(\mathbf{Q}, \omega)$ give the fitted energy positions of the experimental spin wave dispersion.

where bg is the background, $A(\omega, T) = [1 + n(\omega, T)]Z\omega\sigma/2$, $n(\omega, T) = 1/(e^{\omega/k_B T} - 1)$ is the Bose factor, Z is the weight of the excitations, ϵ is their energy, and σ is the half width at half maximum. The resulting energy position of the excitations is reported as black dots in Figs. 2(c)–2(h). All \mathbf{Q} scans have been combined into the experimental maps presented in Figs. 2(c)–2(e). The magnetic nature of the excitations has been checked through the temperature dependence. Well-defined spin waves are observed, as expected for this ordered compound. An acousticlike mode emerging from the antiferromagnetic Bragg position $(1/2, 1/2, 1/2)$ is clearly visible, as well as a high-energy branch along $(h, h, 0)$. Additionally, an almost nondispersive mode located at the energy of about 19 meV is observed along $(2, 2, \ell)$. Higher energy modes are

inferred from Raman spectroscopy with two magnetic excitations identified at the energies 32.2 and 58.5 meV, out of the energy window of our neutron experiments [37].

Our INS measurements were then compared with spin wave calculations performed using the SpinWave software [38,39] based on the linear spin wave theory using the Holstein-Primakoff formalism [40]. The starting point was the model hamiltonian of Eq. (1) involving five isotropic superexchange interactions (see Fig. 1). Two additional constrains were used to limit the number of refined parameters. First, it was shown in [12] that the rotation angle $\alpha = 155^\circ$ between both iron sublattices is obtained for $J_3/J_5 = 2.15$. A second relation between the exchange interactions was inferred from the Curie-Weiss temperature $\theta_{CW} \approx -1670$ K estimated from magnetic susceptibility measurements [12]. We used the local Weiss molecular field model on the stabilized magnetic structure and the equipartition theorem [41]

$$2 \times \frac{3}{2} k_B \theta_{CW} = \mathbf{S}_1 \sum_j J_{1j} \langle \mathbf{S}_j \rangle + \mathbf{S}_2 \sum_j J_{2j} \langle \mathbf{S}_j \rangle, \quad (3)$$

where \mathbf{S}_1 (\mathbf{S}_2) is the spin on site Fe_1 (Fe_2). This allowed us to further reduce the model to three independent parameters, which were systematically varied in the calculations. We checked the capability of each of the sets of parameters to reproduce the measured spin waves, as well as the magnetic structure of $\text{Bi}_2\text{Fe}_4\text{O}_9$ through a real-space mean-field energy minimization of the spin configuration. Finally, a model Hamiltonian compatible with the experiments was obtained with the values of the exchange constants given in Table I. The calculated spin waves are displayed in the lower panels of Figs. 2(f)–2(h) and show a very good agreement with the experimental data. The calculations indicate that the spin waves dispersion extends at higher energies up to 80 meV (see Supplemental Material [29]), with, in particular, two zone center modes at the energy positions of the Raman excitations, which further validates our model.

Our analysis establishes that all five interactions are antiferromagnetic. Because of the geometry of the pentagonal lattice, this implies competition between the J_3, J_4 ,

TABLE I. Values of the antiferromagnetic exchange interactions of $\text{Bi}_2\text{Fe}_4\text{O}_9$ deduced from the INS measurements. The uncertainties on J_1, J_2 , and J_3 are estimated from the standard deviations of the fit of the experimental spin wave dispersion. The J_4 and J_5 uncertainties have been obtained by error propagation: J_5 is imposed by the constraint J_3/J_5 and J_4 by the relation (3).

J (meV)	J_1	J_2	J_3	J_4	J_5
IN22	3.7(2)	1.3(2)	6.3(2)	24.0(8)	2.9(1)

and J_5 interactions within the ab planes confirming the role of magnetic frustration in the stabilization of the 90° magnetic order previously reported [12].

The antiferromagnetic interaction J_1 between the Fe_2 pairs of spins sandwiching the pentagonal planes is actually overcome by an effective ferromagnetic coupling resulting from the interactions of the Fe_2 spins with the Fe_1 spins in the ab planes via J_3 and J_5 . Moreover, this indirect coupling produces the same local field on both Fe_2 spins. This configuration leads to a nearly flat optical mode visible around 19 meV in all directions of reciprocal space and associated with these pairs of Fe_2 spins [see Fig 2(e)]. Along $(1/2, 1/2, \ell)$ and $(h, h, 0)$, this mode was not visible in our experimental data. However, we investigated in purpose the $(2, 2, \ell)$ direction where this mode was strongest in the calculations. We indeed observed it experimentally along this reciprocal space direction. This excited state corresponds to the out-of-phase precession of both Fe_2 spins around their local field, which does not influence the neighboring Fe_1 spins and thus remains localized. A weak dispersion is actually calculated due to the J_2 interplane couplings in the c direction, which is beyond the instrumental resolution of the experiment (see Supplemental Material [29]).

Also noticeable in Table I is the fact that the J_4 interaction is significantly stronger than the other ones, which is compatible with the 180° superexchange path through the central oxygen ion according to the Goodenough-Kanamori rules [42]. This hierarchy of interactions results in a lattice with dominant pairs of antiferromagnetically coupled spins Fe_1 on almost orthogonal bonds [see Fig. 1(a)], a picture that is expected to survive above the Néel temperature. Note that the exchange interactions deduced from our spin wave analysis are slightly different from those obtained from *ab initio* calculations [29,43] in the LSDA + U approximation. However, the positive sign of all exchange couplings (antiferromagnetic) and the overall hierarchy of the interactions are identical in both cases.

In order to investigate the fingerprint of these Fe_1 dimers in the paramagnetic state, we measured the magnetization distributions under a magnetic field of 6 T with two orientations with respect to the crystallographic axes, as shown in Fig. 3. The magnetization per site has been extracted from these maps in the dipolar approximation, implying a spherical electronic distribution around the atoms. Several fitting processes were performed taking into account the presence of magnetic moments on the iron sites only or on all the iron, oxygen, and bismuth sites. A magnetic contribution can indeed be present on the oxygen atoms and, due to their $6s$ lone electron pairs, on the Bi atoms. The final averaged magnetizations per Fe sites are given in Table II.

Interestingly, in the paramagnetic state [Figs. 3(a) and 3(b)], the two iron sites have radically different behaviors:

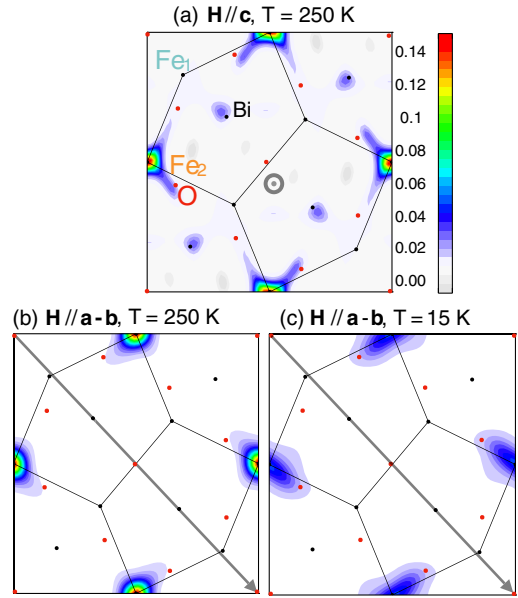


FIG. 3. Spatial distributions of the magnetization of $\text{Bi}_2\text{Fe}_4\text{O}_9$ in μ_B projected along the c axis measured with polarized neutrons under a magnetic field $\mu_0 H = 6$ T applied (a) along c at $T = 250$ K and (b) along $a-b$ at $T = 250$ K, and (c) along $a-b$ at $T = 15$ K.

whereas the Fe_2 ions carry an induced magnetic moment of $0.045(5) \mu_B$ aligned along the field, the induced magnetization on site Fe_1 is vanishingly small (see Table II). This is in contrast with the ordered magnetic moments on both sites refined from previous neutron diffraction experiments below T_N , which are rather similar, equal to 3.52 and $3.73 \mu_B$, respectively [12]. Our measurements, performed with two different directions of the magnetic field, yield the same result, which show that the anisotropy is not responsible for this behavior as expected for Fe^{3+} ions with zero orbital angular momentum. The most noticeable difference between the two maps in Figs. 3(a) and 3(b) is the presence of magnetic density on the Bi sites for $\mathbf{H} \parallel c$ and not for $\mathbf{H} \parallel a-b$. This could be real or an artifact due to an imperfect

TABLE II. Values of the magnetization measured in $\text{Bi}_2\text{Fe}_4\text{O}_9$ at $T = 250$ and 15 K and under a magnetic field $\mu_0 H = 6$ T: macroscopic magnetization m per unit cell (second column) obtained with an extraction magnetometer with the field direction along $a-b$ at 15 K and along $a-b$ or c at 250 K; magnetization per site m_{Fe_1} and m_{Fe_2} (third and fourth columns) deduced from the flipping ratio neutron experiments. At $T = 15$ K the magnetic density was obtained for $\mathbf{H} \parallel a-b$. At $T = 250$ K, the magnetic density is the average of the values obtained for $\mathbf{H} \parallel c$ and $\mathbf{H} \parallel a-b$ since the same macroscopic magnetization is measured.

T (K)	m (μ_B)	m_{Fe_1} (μ_B)	m_{Fe_2} (μ_B)
250	0.220(5)	0.001(5)	0.045(5)
15	0.263(5)	0.014(8)	0.041(7)

reconstruction for $\mathbf{H}\parallel\mathbf{c}$ since a smaller number of observations has been used compared to $\mathbf{H}\parallel\mathbf{a-b}$. The magnetization distribution has also been measured at low temperature [see Fig. 3(c)]. A larger field-induced polarization on the Fe_2 compared to the Fe_1 one is actually preserved in the ordered state. As detailed in Table II, the magnetization on the Fe_1 is actually slightly larger at 15 K than at 250 K and also more delocalized (see Supplemental Material [29]).

These results point to an original paramagnetic state. A calculation assuming free spins $5/2$ in a 6 T field at 250 K yields a field-polarized magnetization of $0.19 \mu_B$, which is 4 times larger and almost 200 times larger than the one measured on the Fe_2 and Fe_1 , respectively. This suggests that, slightly above T_N , the Fe_1 form an assembly of strongly correlated antiferromagnetic dimers in agreement with the dominant J_4 , while the Fe_2 spins are much less correlated. Since the Fe_1 ions form a spin arrangement with great similarities to a Shastry-Sutherland lattice, we suggest that the temperature regime slightly above T_N could be reminiscent of this original physics [15–17]. At higher temperature, the correlations among dimers should vanish, while at lower temperature, correlations involving Fe_2 spins grow, driving the system to the physics of the Cairo pentagonal lattice. Below T_N , the long-range magnetic order is finally triggered by the weakest J_2 interaction, connecting the pentagonal planes. Note that $\text{Bi}_2\text{Fe}_4\text{O}_9$ is not the unique materialization of the Cairo lattice, as it is related to a wide family of compounds including the multiferroic RMn_2O_5 (R a rare-earth/Y, Mn occupying the pentagonal lattice) whose complex magnetodielectric phase diagrams could be investigated in the renewed perspective of pentagonal physics [27,44,45].

Our neutron scattering investigation of $\text{Bi}_2\text{Fe}_4\text{O}_9$ allowed us to achieve a complete determination of its complex magnetic interactions and to unveil various facets of unconventional magnetism, including frustration and dimer physics, with distinct behaviors associated with the two inequivalent Fe sites of the pentagonal lattice. The Fe_1 ions produce strongly coupled antiferromagnetic pairs of spins dominating the correlated paramagnetic state, whereas in the ordered state, the pairs of Fe_2 spins produce original spin dynamics, associated with protected local motions, coexisting with dispersive spin waves. Beyond the canonical examples of frustrated systems, like kagome or pyrochlore lattices with first-neighbor interactions, our Letter discloses novel behaviors that should be more generally observed in materials where the frustration is interlocked with complex connectivity and hierarchical interactions.

We are grateful to J. Debray for the orientation of the sample, the Institut Laue Langevin for providing us with the neutrons, and Navid Qureshi for his help in the data analysis. J. R. thanks B. Canals for the joint development of the software used for the calculations of the spin dynamics

presented in the Supplemental Material [29]. Part of this project was supported by Bulgarian National Science Fund BNSF DN–08/9.

*Current address: Institut Laue Langevin, 38000 Grenoble, France.

beauvois@ill.fr

†virginie.simonet@neel.cnrs.fr

- [1] R. Ballou, *J. Alloys Compd.* **275–277**, 510 (1998).
- [2] R. Moessner and A. P. Ramirez, *Phys. Today* **59**, No. 2, 24 (2006).
- [3] L. Balents, *Nature (London)* **464**, 199 (2010).
- [4] R. Moessner and K. S. Raman, in *Introduction to Frustrated Magnetism*, edited by C. Lacroix, P. Mendels, and F. Mila (Springer, Berlin, 2011), Vol. 164.
- [5] J. Robert, B. Canals, V. Simonet, and R. Ballou, *Phys. Rev. Lett.* **101**, 117207 (2008).
- [6] K. Matan, D. Grohol, D. G. Nocera, T. Yildirim, A. B. Harris, S. H. Lee, S. E. Nagler, and Y. S. Lee, *Phys. Rev. Lett.* **96**, 247201 (2006).
- [7] K. Tomiyasu, H. Suzuki, M. Toki, S. Itoh, M. Matsuura, N. Aso, and K. Yamada, *Phys. Rev. Lett.* **101**, 177401 (2008).
- [8] M. E. Zhitomirsky, *Phys. Rev. B* **78**, 094423 (2008).
- [9] S. T. Bramwell and M. J. P. Gingras, *Science* **294**, 1495 (2001).
- [10] L. Savary and L. Balents, *Rep. Prog. Phys.* **80**, 016502 (2017).
- [11] A. Kitaev, *Ann. Phys. (N.Y.)* **321**, 2 (2006).
- [12] E. Ressouche, V. Simonet, B. Canals, M. Gospodinov, and V. Skumryev, *Phys. Rev. Lett.* **103**, 267204 (2009).
- [13] K. S. Raman, R. Moessner, and S. L. Sondhi, *Phys. Rev. B* **72**, 064413 (2005).
- [14] I. Rousochatzakis, A. M. Läuchli, and R. Moessner, *Phys. Rev. B* **85**, 104415 (2012).
- [15] B. S. Shastry and B. Sutherland, *Physica (Amsterdam)* **B +C108**, 1069 (1981).
- [16] C. H. Chung, J. B. Marston, and S. Sachdev, *Phys. Rev. B* **64**, 134407 (2001).
- [17] P. A. McClarty, F. Krüger, T. Guidi, S. F. Parker, K. Refson, A. W. Parker, D. Prabhakaran, and R. Coldea, *Nat. Phys.* **13**, 736 (2017).
- [18] F. C. Rodrigues, S. M. de Souza, and O. Rojas, *Ann. Phys. (N.Y.)* **379**, 1 (2017).
- [19] V. Urumov, *J. Phys. A* **35**, 7317 (2002).
- [20] M. Rojas, O. Rojas, and S. M. de Souza, *Phys. Rev. E* **86**, 051116 (2012).
- [21] H. Nakano, M. Isoda, and T. Sakai, *J. Phys. Soc. Jpn.* **83**, 053702 (2014).
- [22] M. Isoda, H. Nakano, and T. Sakai, *J. Phys. Soc. Jpn.* **83**, 084710 (2014).
- [23] K. Karlova, J. Strecka, and M. L. Lyra, *Phys. Rev. B* **97**, 104407 (2018).
- [24] A. Ralko, *Phys. Rev. B* **84**, 184434 (2011).
- [25] A. M. Abakumov, D. Batuk, A. A. Tsirlin, C. Prescher, L. Dubrovinsky, D. V. Sheptyakov, W. Schnelle, J. Hadermann, and G. Van Tendeloo, *Phys. Rev. B* **87**, 024423 (2013).

- [26] A. A. Tsirlin, I. Rousochatzakis, D. Filimonov, D. Batuk, M. Frontzek, and A. M. Abakumov, *Phys. Rev. B* **96**, 094420 (2017).
- [27] S. Chattopadhyay, S. Petit, E. Ressouche, S. Raymond, V. Balédent, G. Yahia, W. Peng, J. Robert, M.-B. Lepetit, M. Greenblatt, and P. Foury-Leylekian, *Sci. Rep.* **7**, 14506 (2017).
- [28] J. Cumby, R. D. Bayliss, F. J. Berry, and C. Greaves, *Dalton Trans.* **45**, 11801 (2016).
- [29] See Supplemental Material at <http://link.aps.org/supplemental/10.1103/PhysRevLett.124.127202> for details on the magnetization density maps, spin waves analysis, comparison with *ab initio* calculations, quasiflat excitation, and presentation of spin dynamics calculations of the magnetic structure factor, which includes Refs. [30–34].
- [30] J. C. Matthewman, P. Thompson, and P. J. Brown, *J. Appl. Crystallogr.* **15**, 167 (1982).
- [31] J. Skilling and S. F. Gull, in *Maximum Entropy and Bayesian Methods in Inverse Problems*, edited by C. R. Smith and W. T. Grandy, Jr. (Springer, Dordrecht, 1985), p. 83.
- [32] B. Himmetoglu, A. Floris, S. de Gironcoli, and M. Cococcioni, *Int. J. Quantum Chem.* **114**, 14 (2014).
- [33] M. Taillefumier, J. Robert, C. L. Henley, R. Moessner, and B. Canals, *Phys. Rev. B* **90**, 064419 (2014).
- [34] J. Robert, E. Lhotel, G. Remenyi, S. Sahling, I. Mirebeau, C. Decorse, B. Canals, and S. Petit, *Phys. Rev. B* **92**, 064425 (2015).
- [35] T. Weber, R. Georgii, and P. Böni, *SoftwareX* **5**, 121 (2016).
- [36] T. Weber, *SoftwareX* **6**, 148 (2017).
- [37] M. N. Iliev, A. P. Litvinchuk, V. G. Hadjiev, M. M. Gospodinov, V. Skumryev, and E. Ressouche, *Phys. Rev. B* **81**, 024302 (2010).
- [38] S. Petit, *Numerical Simulations and Magnetism*, Collection SFN (EDP Sciences, 2011), Vol. 12, pp. 105–121, <https://doi.org/10.1051/sfn/201112006>.
- [39] <http://www-llb.cea.fr/logicielsllb/SpinWave/SW.html>.
- [40] T. Holstein and H. Primakoff, *Phys. Rev.* **58**, 1098 (1940).
- [41] R. M. White, *Quantum Theory of Magnetism*, Springer in Solid State Science (Springer, Berlin, Heidelberg, 2007).
- [42] J. B. Goodenough, *Magnetism and the Chemical Bond* (John Wiley and Sons, New York, 1963).
- [43] Z. V. Pchelkina and S. V. Streltsov, *Phys. Rev. B* **88**, 054424 (2013).
- [44] P. G. Radaelli and L. C. Chapon, *J. Phys. Condens. Matter* **20**, 434213 (2008).
- [45] W. Peng, V. Balédent, C. V. Colin, T. C. Hansen, M. Greenblatt, and P. Foury-Leylekian, *Phys. Rev. B* **99**, 245109 (2019).